JAERI-M
85-117

ANALYSIS OF TRAC-PF1 CALCULATED CORE HEAT TRANSFER FOR CCTF TEST C1-5 (RUN 14)

August 1985

Hajime AKIMOTO

日本原子力研究所
Japan Atomic Energy Research Institute

JAERI-M レポートは，日本原子力研究所が不定期に公刊している研究報告書です。
入手の問合わせは，日本原子力研究所技術情報部情報資料課（〒319--11 茨城県那珂郡東海村）あて，お申しこしください。なお，このほかに財団法人原子力弘済会資料センター（〒319-11 茨城県那珂郡東海村日本原子力研究所内）で複写による実費頒布をおこなっております。

JAERI-M reports are issued irregularly.
Inquiries about availability of the reports should be addressed to Information Division, Department of Technical Information, Japan Atomic Energy Research Institute, Tokai-mura, Naka-gun, Ibaraki-ken 319-11, Japan.

編集兼発行　日本原子力研究所
印　　刷　山田軽印刷所

JAERI-M 85-117

Analysis of TRAC-PF1 calculated core heat transfer for CCTF test C1-5 (Run 14)

Hajime AKIMOTO

Department of Reactor Safety Research,
Tokai Research Establishment, JAERI

(Received July 17, 1985)

A TRAC-PF1 post test calculation for CCTF test C1-5 (Run 14) was performed to assess the core thermal-hydraulic models in the TRAC-PF1 code during the reflood phase of a PWR LOCA. TRAC showed good agreement with data for heater rods turnaround temperatures and turnaround times in the lower half of the core. However, TRAC overpredicted turnaround times and underpricted quench times in the upper part of the core. Even though heat transfer correlations have a strong dependency on the local void fraction in TRAC, TRAC-predicted void fraction profile showed poor agreement with CCTF data that have been inferred from differential pressure measurements. TRAC predicted a step change of void fraction at the collapsed water level, while CCTF results showed a continuous profile of void fraction in the core. From these comparisons with CCTF data, the following areas for future improvements of TRAC-PF1 should be considered: (1) the core hydraulic modeling used to calculate the void fraction profile in the core (2) the method for evaluating heat transfer within the core.

Keywords: Reactor Safety, Loss-of-coolant, PWR, Reflood, CCTF, TRAC Code, Two-phase Flow, Heat Transfer, Comparative Evaluation

---

The work was performed under contract with the Atomic Energy Bureau of Science and Technology of Japan.

JAERI-M 85-117

円筒炉心試験C1−5(Run 14)に対するTRAC−PF1コードによる炉心熱伝達計算の検討

日本原子力研究所東海研究所原子炉安全工学部
秋　本　　肇

(1985年7月17日受理)

加圧水型原子炉冷却材喪失事故再冠水時におけるTRAC−PF1コードの炉心内熱水力モデルを評価する目的で円筒炉心試験C1−5(Run 14)に対するTRAC−PF1コードによる試験後解析を行った。炉心下半分では，加熱棒のターンアラウンド温度とターンアラウンド時間について，実験と解析のよい一致がみられた。しかしながら，炉心上半分では，TRACコードはターン アラウンド時間を長めにクエンチ時間を短かめに評価した。TRACコードでは熱伝達相関式が局所ボイド率に対する強い依存性を有するにもかかわらず，TRACコードで予測されたボイド率と差圧測定より求めた円筒炉心試験データとの一致は悪かった。すなわち，円筒炉心試験結果では炉心内で連続的なボイド率分布が観察されているのに対し，TRACコードはコラプスト水位でのステップ状変化を伴なうボイド率分布を予測した。これらの円筒炉心試験結果との比較結果は，以下の領域で今後TRAC−PF1コードの改良が必要なことを示す。(1)炉心内ボイド率分布計算に係る炉心内水力モデル (2) 炉心内の熱伝達評価方法

本報告書は，電源開発促進対策特別会計法に基づき，科学技術庁からの受託によって行われた研究の成果である。

Contents

目　　次

1. Introduction

The Transient Reactor Analysis Code (TRAC) is being developed at the Los Alamos National Laboratory to provide advanced best-estimate predictive analyses of postulated accidents in light water reactors.[1] TRAC-PF1 which was released in November 1981 was used to perform the analysis reported. TRAC-PF1 was designed to improve the capability of TRAC-PD2[2] and to include all of the major improvements of TRAC-PD2.

TRAC provides analysis support to a multinational experimental and analytical research program (known as 2D/3D program) investigating multidimensional thermal-hydraulic behavior during loss-of-coolant accidents in pressurized water reactors. The test analysis with TRAC-PF1 code was started at Los Alamos in 1982.

The Cylindrical Core Test Facility (CCTF) provides information on thermal-hydraulic behavior during the refill and reflood phases of a loss-of-coolant accident in a pressurized water reactor[3],[4]. CCTF has full-height core section with about 2000 electrically heated rods arranged in a cylindrical configuration and has four primary loops with active steam generators and reactor component simulators. The system integral effects and the cooling characteristics of the core are being investigated to demonstrate the effectiveness of the emergency core-cooling system (ECCS), to verify computer codes, and to collect information to improve the thermal-hydraulic models in analysis codes.

The objective of this report is to assess the TRAC-PF1 core heat transfer model during the reflood phase of a loss-of-coolant accident of a pressurized water reactor (PWR) by analyzing the core cooling behavior for the CCTF test C1-5 (Run 14)[4]. A simplified model of only the core and part of the upper and lower plena is used. Measured core inlet mass flow and fluid temperature are applied as boundary conditions. The calculated rod temperature histories, heat transfer coefficients, and void fractions are compared with the test data to assess the thermal-hydraulic models in TRAC-PF1.

2. TRAC input

Version 8.2 of TRAC-PF1 was used in this study because this version was used for analysis of several CCTF tests. Figure 1 shows the system noding. Only the core and the upper plenum of CCTF are modeled to assess the core thermal-hydraulic model of the TRAC-PF1 code. The core inlet boundary conditions are specified by a FILL component with time-dependent core inlet mass flow and fluid temperature. The core outlet boundary conditions are specified by two BREAK components with time-dependent pressures.

Figure 2 shows the noding schematic of the VESSEL component. The CCTF core and upper plenum are modeled with 1 radial ring, 2 azimuthal sectors, and 14 levels. Data used for modeling of the CCTF geometry is shown in Table 1. Table 1 summarizes the TRAC input data for cell volume, hydraulic diameter, flow area, and heat slab area. The core extends axially from the second level to the eighth level. Two supplemental rods are included to simulate the high-power rod in the higher-power region and the medium-power rod in the medium-power region. The peaking factors of these rods relative to the core average power are 1.2659 and 1.0920, respectively. The inlet FILL component is connected to the first axial cell. Each BREAK component is connected to the thirteenth axial level.

Figure 3 shows the comparisons of the core inlet mass flow rate, which was derived by a mass balance calculation[4]. For this calculation, a flow of 23.5 kg/s is assumed during the accumulator injection period (63 s < t < 74 s) and 5.03 kg/s is assumed during the low-pressure injection period (78 s < t). The assumed mass flow rate resulted in good agreement with the total core inlet mass flow as shown in Fig. 4.

Figure 5 shows the comparison of the measured core inlet fluid temperature to the imposed temperature. The calculated core inlet fluid temperature agrees with test data.

Figure 6 and 7 show the comparisons of the upper plenum pressure and the core power, respectively. Both show good agreement with test data.

The calculated results show excellent agreement with test data for the core inlet mass flow rate and fluid temperature, the upper plenum pressure, and the core power. This makes it possible to assess the core thermal-hydraulic and heat transfer models in detail because the differences between the calculated and measured results should be

caused by the differences between the models and the actual phenomena.

Table 1 Revised geometry for CCTF vessel

LEVEL	VOL(m^3)	HD(Z)(m)	HD(θ)(m)	FA(Z)(m^2)	FA(θ)(m^2)	HSA(m^2)
1	0.01000	0.00646	1.0	0.12637	1.0	0.0
2	0.58472	0.012462	0.006344	0.58472	0.2280	1.159
3	0.58472	0.012462	0.006344	0.58472	0.2280	2.318
4	0.58472	0.012462	0.006344	0.58472	0.2280	2.318
5	0.58472	0.012462	0.006344	0.58472	0.2280	2.318
6	0.58472	0.012462	0.006344	0.58472	0.2280	2.318
7	0.58472	0.012462	0.006344	0.58472	0.2280	2.318
8	0.58472	0.012462	0.006344	0.58472	0.2280	1.159
9	0.58472	0.012462	0.006344	0.58472	0.2280	0.456
10	1.29000	0.082855	0.2815	0.3593	0.6827	0.5083
11	1.2681	0.17808	0.07209	1.2681	0.2157	1.8970
12	1.4407	0.1844	0.07209	1.4407	0.2157	2.775
13	1.4407	0.1844	0.07209	1.4407	0.2157	1.983
14	1.4407	0.0	0.07209	0.0	0.2157	5.611

Note: VOL - cell volume
HD(Z) - hydraulic diameter (axial)
HD(θ) - hydraulic diameter (angular)
FA(Z) - flow area (axial)
FA(θ) - flow area (angular)
HSA - heat slab area

Note: On each level both fluid cell have indentical geometry.

3. Results and discussion

3.1 Rod surface temperatures

Figure 8 shows comparisons of rod surface temperature histories along a high-power rod in the high-power region. The reflood phase was initiated at 63 s. The core inlet mass flow was 23.5 kg/s by 74 s and 5.03 kg/s after 78 s, as shown in Fig. 3. The calculated results agree better with the test data in the lower part of the heater rod than on the upper part. This has been generally true in other TRAC analysis of CCTF data[5]. The rod turnaround temperatures, turnaround times, and quench times were selected to assess the capability of the TRAC-PF1 to predict the overall core-cooling characteristics. Figures 9 through 11 show the comparisons of turnaround time and temperature, and quench time between the TRAC-PF1 calculation and the CCTF test data. The comparisons were made for two kinds of heater rods, i.e. the high-power rods in the high-power region and the medium-power rods in the medium power region. The former is the peak powered rod in the CCTF core and is expected to give the peak clad temperature. The latter is the standard rod in the CCTF and can indicate the average temperature in the core. The turnaround and quench times are defined from the start of reflood. Figure 9 shows the comparison of turnaround temperature between TRAC and CCTF results. TRAC prediction shows good agreement with the CCTF test data, especially in the lower part of the core. Figure 10 shows the comparison of turnaround time between the TRAC and the CCTF results. The TRAC results show excellent agreement in the lower part of the core ($Z < 2.0$ m). However, TRAC-PF1 overestimates the turnaround time in the upper part of the core ($2.0 < Z < 3.0$ m). Figure 11 shows the comparison of quench time between the TRAC and the CCTF results. The TRAC results predict early quench times, especially in the upper part of the core ($2.0 < Z < 3.0$ m). These results show that TRAC can predict the overall rod cooling characteristics well. However, some revisions in the TRAC models to represent cooling in the upper part of the core should be made because it overpredicted the turnaround time and underpredicted the quench time in this region.

3.2 Wall-to-fluid heat transfer coefficients

The TRAC code estimates the wall-to-fluid heat transfer coefficient in terms of the two-phase flow regimes. Figure 12 shows the wall-to-fluid

heat transfer regime for the peak powered rod. The single-phase flow, the nucleate boiling, the transition boiling, and the film boiling regimes are used to evaluate the wall-to-fluid heat transfer coefficients. The calculated turnaround time and quench front positions are indicated in Fig. 12. The turnaround temperature is predicted to occur in the film boiling regime except at the top part of the core ($Z > 3.3$ m) where the rod surface temperature was low. The bottom flooding quench front coincides with the boundary between the nucleate and film boiling regimes. Figure 12 shows that the heat transfer regime on the unquenched part of the rod is film boiling. This result suggests that the most important heat transfer correlations is the film boiling regime during the reflood phase. The heat transfer correlations used to evaluate the film boiling regime in TRAC-PF1 are summarized in Appendix A. The liquid heat transfer coefficient h_ℓ is evaluated by the summation of the radiative contribution h_r, the dispersed flow heat transfer coefficient h_{df}, and the Bromley film-boiling heat transfer coefficient h_{fbb}. Each h_r, h_{df}, and h_{fbb} is expressed as a function of $(1 - \alpha)$. The gas heat transfer coefficient h_g is evaluated by the maximum of the turbulent natural-convection heat transfer coefficient h_{nc} and the forced-convection heat transfer coefficient h_{fc}.

Figure 13 shows the calculated profiles of the void fraction and the heat transfer coefficients at 223 s after the reflood initiation. The calculated heat transfer regimes are shown in this figure. The nucleate boiling regime is used below 1.64 m and the transition boiling regime is used between 1.64 and 1.67 m. At the top of the heater rod, the heat transfer coefficient is calculated to be transition boiling because of low wall temperature due to the low power at this elevation. The quench front position at this time is located at 1.64 m in the transition boiling regime. The calculated collapsed water level is in the fifth fluid cell and its elevation is 2.293 m. A void fraction of 0.2 is used to calculate the heat transfer coefficient below this level, while a void fraction of 0.9985 is used above this level. The rapid change of h_ℓ is evident at the elevation of the collapsed water level. In the calculation, the heat transfer to the liquid is significant below the collapsed water level and the heat transfer to the steam is significant above the collapsed water level. This result can be related to the abrupt void fraction change at the collapsed water level.

Table 2 shows the comparison of the wall-to-fluid heat transfer

coefficients below and above the collapsed water level at 223 s after the reflood initiation. The heat transfer is calculated for each heat conduction fine mesh cells. Cells above and below the collapsed water level were selected for comparison. Liquid heat transfer coefficient reduces from 238.77 $W/(m^2-K)$ to 0.164 $W/(m^2-K)$ as the collapsed water level is crossed. Because these two cells are located in the same fluid cell, the same values of thermal-hydraulic diameter, pressure, fluid properties, and velocities are used to calculate the heat transfer coefficient at the two locations in TRAC.

Below the collapsed water level, the predicted void fraction is 0.2 and results in the high h_{fbb} as shown in Appendix A. The radiative contribution is proportional to $(1 - \alpha)$, and gives a rather high heat transfer coefficient below the collapsed water level. The predicted void fraction above the collapsed water level is 0.9985, both h_{fbb} and h_r reduce because of the high void fraction, as shown in Table 2.

Gas heat transfer coefficient is evaluated by the maximum of the natural and forced-convection heat transfer coefficients. The forced-convection heat transfer coefficient is higher than natural-convection heat transfer coefficient in this case.

As shown by Eq. (A-11), h_g is a function of the two-phase mixture velocity. By changing α from 0.2 to 0.9985, the velocity increases from 1.676 m/s to 7.196 m/s. This results in an increased gas heat transfer coefficient from 24.91 $W/(m^2-K)$ to 79.92 $W/(m^2-K)$. These results indicate the following TRAC prediction tendencies;

1. The wall-to-fluid heat transfer coefficient has a strong dependency on the void fraction and on the location of the collansed water level.
2. Below the collapsed water level, heat transfer to liquid is dominant. Heat transfer to gas is only one-tenth of that to liquid.
3. Above the collapsed water level, heat transfer to liquid is negligible because of the high void fraction.
4. By crossing the collapsed water level, the total heat transfer to gas and liquid increases because of increase in the liquid heat transfer coefficient.

Figure 14 shows the comparison of the wall heat transfer coefficient at the midplane of the high-power rod in the high-power region. CCTF data have been used to derive heat transfer coefficients from

the measured clad surface temperature transient using an inverse heat-conduction technique[6]. The CCTF heat transfer coefficient is evaluated based on the local saturation temperature. Because TRAC evaluates heat transfer coefficients based on the local steam and water temperature, TRAC-calculated heat transfer coefficients were modified to compare with the CCTF heat transfer coefficients using the following relations:

$$q_\ell = h_\ell (T_w - T_\ell) = h_\ell^* (T_w - T_{sat}) \quad , \tag{1}$$

$$q_g = h_g (T_w - T_g) = h_g^* (T_w - T_{sat}) \quad . \tag{2}$$

These modified heat transfer coefficients h_ℓ^* and h_g^* are shown in Fig. 14. Calculated results show an abrupt change around 80 s. This is due to the passing of the collapsed water level at this time. Before the arrival of the collapsed water level, calculated heat transfer coefficient shows good agreement with test data. This result is consistent with the good agreement obtained in the turnaround time and temperature at the midplane. After the collapsed water level passes, the heat transfer to water is significantly higher in TRAC. The calculated water heat transfer coefficient is about twice that indicated by the CCTF results. These comparisons indicate TRAC overpredicts cooling of the heater rods after the collapsed water level passes. This result is consistent with the shorter quench time calculated by TRAC as compared to CCTF results.

Table 2 Comparison of wall-to-fluid heat transfer coefficient around the collapsed water level

(a) Liquid heat transfer coefficient h_ℓ (W/m^2K)

	Below the collapsed level (2.250 m)	Above the Collapsed level (2.364 m)
h_ℓ (*1)	238.77	0.164
$h_r\left(\frac{T_w - T_s}{T_w - T_\ell}\right)$ (*2)	69.60	0.134
h_{df} (*3)	2.05	0.029
h_{fbb} (*4)	167.12	0.000
Void fraction	0.2	0.9985

Note: (*) Collapsed water level = 2.293 m.
(*1) Liquid heat transfer coefficient, [see Eq. (A-5)].
(*2) Radiative contribution [see Eq. (A-6)].
(*3) Dispersed flow HTC [see Eq. (A-7)].
(*4) Bromley film-boiling HTC [see Eq. (A-8)].

(b) Gas heat transfer coefficient h_g (W/m^2K)

	Below the collapsed level (2.250 m)	Above the Collapsed level (2.364 m)
h_g (*5)	24.91	79.92
h_{nc} (*6)	20.35	20.50
h_{fc} (*7)	24.91	79.92
$\alpha V_g + (1-\alpha)V_\ell$ (*8)	1.676	7.196

Note: (*5) Gas heat transfer coefficient [see Eq. (A-9)].
(*6) Natural convection HTC [see Eq. (A-10)].
(*7) Forced convection HTC [see Eq. (A-11)].
(*8) Two-phase mixture velocity in Eq. (A-11).

3.3 Core Hydraulic Behavior

Figure 15 shows a comparison of the void fraction profile in the core at 37, 137, and 237 s after the reflood initiation for the TRAC-PF1 prediction and CCTF measurement (inferred from differential pressure). The TRAC prediction shows poor agreement with CCTF data. TRAC predicts a step change of void fraction at the collapsed water level, which is not evident in the CCTF data. This result suggests a qualitative difference between the TRAC hydraulic model and CCTF results. CCTF results show the quick spreading of water to the top of core right after the reflood initiation. A nearly constant void fraction ($\alpha = 0.8$ to 0.9) is maintained through the remainder of the transient. On the contrary, the TRAC prediction is characterized by the propagation of the collapsed water level with the low void fraction (less than 0.2) below the collapsed water level and high void fraction (more than 0.99) above the quench front. It should be noted that the wall-to-fluid heat transfer coefficient has a strong dependency on the local void fraction. Therefore, these results indicate a future improvement on the core hydraulic model should be considered.

Below the collapsed water level, the predicted void fraction is less than 0.2. This means that TRAC calculations are based on the bubbly flow correlations. CCTF results indicate a higher void fraction at the same elevation. The TRAC interfacial drag model for the bubbly flow may underpredict the interfacial drag. Review of the interfacial drag correlation is recommended as a future improvement of TRAC-PF1. Above the collapsed water level, TRAC predicts a higher void fraction than indicated by CCTF results. CCTF results show the void fraction above the collapsed water level to be about 0.8 to 0.9. This suggests that slug flow or churn-turbulent flow is established in the upper part of the core. But TRAC calculates dispersed flow or droplet flow above the collapsed water level. Drops are accelerated quickly and the high void fraction is predicted in TRAC. Again, this indicates the drag model should be reviewed. The precursory cooling evaluation is one of the most important factors for predicting the turnaround temperature and the void fraction is one of the most important parameters in predicting the wall-to-fluid heat transfer coefficient. Therefore, it is essential to select an accurate correlation to predict the void fraction distribution. It also recommended that a review be made of the assumption that droplet flow occurs above the collapsed water level.

Figure 16 shows the comparison of the accumulated core mass between TRAC-PF1 and CCTF data. TRAC overestimates the water accumulation rate in the core. The predicted core mass is about 200 kg higher than the CCTF data at 300 s. As shown in Fig. 15, TRAC underestimates the void fraction below the collapsed water level and overestimates it above the collapsed water level. Figure 16 shows the overprediction below the collapsed water level has a significant effect on the total core mass. It is also evident that the present TRAC-PF1 model underpredicts the total core outlet mass flow; this is an essential parameter in calculating the steam binding effect during the reflood. The discrepancy in the core outlet mass flow rate will result in an underestimation steam binding effects if a system analysis is performed with an upper plenum and loop model.

Figure 17 shows the relation of the turnaround time along the high-power rod in the high-power region with the collapsed water level in the TRAC calculation. Turnaround at each elevation is well correlated with the time when the collapsed water level passes through the elevation. Stationary behavior of the collapsed water level is realized at 2.135 and 2.745 m. These elevations coincide with the heights of the fluid cell boundaries. It seems that this stationary behavior is caused by the code model used at hydro-cell interfaces rather than by physical reasons. Wall-to-fluid heat transfer coefficient in the fine-mesh cell is evaluated with the bottom or the cell center value of the coarse fluid cell. When the collapsed water level moves to the next fluid cell, a discontinuous change occurs in the evaluation of the wall-to-fluid heat transfer. This produces unrealistic behaviors of the collapsed water level at the fluid cell boundaries. Special modeling is used in the code at cell boundaries and more studies of this model behavior are necessary to improve the transition from level to level.

4. Conclusions

A TRAC-PF1 calculation (Version 8.2) for CCTF test C1-5 (Run 14) was performed to assess the core thermal-hydraulic models in the TRAC-PF1 code during the reflood. Through comparisons with test data, the following conclusions were obtained.

1. TRAC shows good agreement with data for the heater rods turnaround temperatures and turnaround times in the lower half of the core. However, TRAC overpredicted turnaround times and underpredicted quench times in the upper part of the core.
2. TRAC predicts wall-to-fluid heat transfer coefficients with single-phase flow, nucleate boiling, transition boiling, and film-boiling-regime correlations. Most of the heat transfer coefficients in the unquenched region are evaluated with correlations for film-boiling.
3. Heat transfer correlations for the film-boiling-regime have a strong dependency on local void fraction.
4. TRAC-predicted void fraction profile showed poor agreement with CCTF data that have been inferred from differential pressure measurements. TRAC predicted a step change of void fraction at the collapsed water level, while CCTF results showed a continuous profile of void fraction in the core.

5. Recommendations

From these comparisons with CCTF test data, the following areas for future improvements of the TRAC-PF1 should be considered:

1. Review the core hydraulic modeling used to calculate the void fraction distribution in the core.
2. Review the heat transfer correlations for the film-boiling regime, especially the dependency on local void fraction.
3. Review the assumption that droplet flow occurs above the collapsed water level.

Acknowledgments

This work was performed during the stay at Los Alamos National Laboratory (LANL) where the author was delegated as a resident engineer in the 2D/3D program since February 1982 to March 1983. He would like to thank Dr. K. Williams, Messrs. R. Fujita, F. Motley, M. Cappiello and Mrs. S. Smith of Los Alamos National Laboratory for their helpful advice. Grateful thanks are forwarded to Mr. F. Motley, for providing support and valuable discussions.

He would like to express his thanks to Drs. M. Nozawa, K. Hirano, M. Shiba, and Y. Murao of JAERI for their guidance and encouragement.

He also appreciates to the members of the CCTF analysis group, Messrs. T. Iguchi, T. Sudoh, J. Sugimoto and T. Okubo for valuable discussions.

References

(1) Liles, D. et al.: "TRAC-PF1: An advanced best-estimate computer program for pressurized water reactor analysis," Los Alamos National Laboratory report (to be published).

(2) Liles, D. et al.: "TRAC-PD2: An advanced best-estimate computer program for pressurized water reactor loss-of-coolant accident analysis, "Los Alamos National Laboratory report LA-8709-MS, NUREG/CR-2054 (April 1981).

(3) Hirano, K. and Murao, Y.: "Large scale reflood test," J. At. Energy Soc. of Japan, 22(10) pp. 681, (1980), (in Japanese).

(4) Murao, Y. et al.: "Experimental study of system behavior during reflood of PWR-LOCA using CCTF," J. Nucl. Sci. and Technol., 19(9) pp. 705, (1982).

(5) Kirchner, W.L. and Williams, K.A.: "FY 1981 2D/3D analysis program annual report," LA-2D/3D-TN-81-36, (1981).

(6) Sugimoto, J. et al.: "Data report on reflood experiment," JAERI-M 8169, (1979), (in Japanese).

Nomenclature

C_p : Specific heat (J/kg)
k : Thermal conductivity (W/mK) or Cell number suffix
D_h : Hydraulic diameter (m)
g : Acceleration of gravity (m/s^2)
h : Heat transfer coefficient (W/m^2K)
h'_{fg}: Latent heat (J/kg)
p : Pressure (Pa)
Pr : Prandl number
q : Heat flux (W/m^2)
T : Temperature (K)
V : Velocity (m/s)
Z : Elevation (m)
α : Void fraction
ρ : Density (kg/m^3)
μ : Viscosity (Pa·s)
σ : Surface tension (N/m)

Suffix

g : Gas
j : Cell number
ℓ : Liquid
L : Index for lower cell
m : Two-phase mixture
q : Collapsed water level
s : Saturation
U : Index for upper cell
W : Wall

Appendix A
Heat transfer correlations for the film boiling regime in TRAC PF1 code (version 8.2)

The film-boiling regime is calculated on in the TRAC-PF1 code if the following conditions are satisfied:

$$T_w > T_{min} \quad , \tag{A-1}$$

where T_{min} is the minimum film boiling temperature evaluated by

$$T_{min} = F(p) \quad . \tag{A-2}$$

the heat fluxes to gas and liquid are evaluated separately by

$$q_\ell = h_\ell \ (T_w - T_\ell) \tag{A-3}$$

and

$$q_g = h_g \ (T_w - T_g) \quad . \tag{A-4}$$

The liquid heat transfer coefficient h_ℓ is evaluated as the sum of the radiative contribution h_r, the dispersed-flow heat transfer coefficient h_{df}, and the Bromley film-boiling heat transfer coefficient h_{fbb}, i.e.

$$h_\ell = h_r \left(\frac{T_w - T_s}{T_w - T_\ell} \right) + h_{df} + h_{fbb} \quad . \tag{A-5}$$

h_r, h_{df}, and h_{fbb} are calculated by the following correlations, respectively:

$$h_r = (1 - \alpha)\sigma\varepsilon \left(\frac{T_w^4 - T_s^4}{T_w - T_s} \right) \quad , \tag{A-6}$$

where σ is the Stefan-Boltzmann constant and ε is the wall emissivity;

$$h_{df} = 0.2 \ C_1 \ [(1 - \alpha)E]^{0.6667} BRAC^{0.25} \left(\frac{T_w - T_s}{T_w - T_\ell} \right) \tag{A-7}$$

where

$$BRAC = \frac{g\rho_\ell \rho_g h'_{\ell g} k_g^3}{(T_w - T_s)\mu_g d_{drop}} \qquad C_1 = 1.2760,\ W_e = 4.0$$

$$d_{drop} = \frac{We\sigma}{\rho_g (V_g - V_\ell)^2} \qquad (1.0 \times 10^{-4} \leqslant d_{drop} \leqslant 3.0 \times 10^{-3}\ \text{m})$$

$$E = \begin{cases} 1.0 - \exp 0.23\,[-(V_g - V_E)], & \text{if } V_g > V_E, \\ \text{or} & \\ 0 \qquad\qquad\qquad\qquad\qquad\qquad & \text{if } V_g \leqslant V_E, \end{cases}$$

$$V_E = 3.65 \left[\frac{(\rho_\ell - \rho_g)\sigma}{\rho_g^2}\right]^{1/4} \quad ;$$

$$h_{fbb} = \begin{cases} h_{fbb0} & (\alpha \leqslant 0.5) \\ (3 - 2X_1)X_1^2 h_{fbb0} & [0.5 < \alpha < 0.75,\ X_1 = \dfrac{0.75 - \alpha}{0.75 - 0.50}] \\ 0 & (0.75 \leqslant \alpha) \end{cases} \qquad \text{(A-8)}$$

where

$$h_{fbb0} = 0.62 \left[\frac{\rho_g k_g^3 (\rho_\ell - \rho_g) g h'_{\ell g}}{\mu_g (T_w - T_s)\lambda}\right]^{1/4}, \quad \lambda = 2\pi \left[\frac{\sigma}{g(\rho_\ell - \rho_g)}\right]^{1/2}.$$

The gas heat transfer coefficient h_g is evaluated by the maximum of the turbulent natural-convection heat transfer coefficient h_{nc} and the forced-convection heat transfer coefficient h_{fc}, i.e.

$$h_g = \max\,(h_{nc},\ h_{fc}) \quad , \qquad \text{(A-9)}$$

where

$$h_{nc} = 0.13\ k_g \left(\frac{\rho_g^2 g[T_w - T_g]}{\mu_g^2 T_g}\right)^{0.333} Pr_g^{0.333} \quad , \qquad \text{(A-10)}$$

$$h_{fc} = 0.023 \frac{k_g}{D_h} \left[\frac{\rho_g [\alpha V_g + (1-\alpha) V_\ell] D_h}{\mu_g} \right]^{0.8} \left[\frac{\mu_g (c_p)_g}{k_g} \right]^{0.4} . \quad \text{(A-11)}$$

In TRAC-PF1, some values are defined at the cell boundary and others are defined at the cell center. Figure A-1 shows values used in the calculation of the heat transfer coefficients. The suffixes j and j±1/2 stand for the cell-center value and the cell-boundary value, respectively. Cell bottom values $Y_{j-1/2}$ are used for fluid velocities. The cell top value $Y_{j+1/2}$ is not used in TRAC-PF1 code version 8.2. Cell-center values X_j are used for thermal-hydraulic diameter, pressure, fluid temperature, and fluid properties. Values from the fine-mesh node are also used for rod surface temperature. Rod properties at the elevation Z are evaluated with a linear interpolation using the data at $Z_{j-1/2}$ and $Z_{j+1/2}$. The void fraction α is evaluated by the following equations:

$$\alpha = \begin{cases} \alpha_j & \text{(If } Z_q \text{ is not in the fluid cell)} \\ \alpha_L & \text{(If } Z_q \text{ is in the fluid cell and } Z_k < Z_q\text{)} \\ \alpha_U & \text{(If } Z_q \text{ is in the fluid cell and } Z_k > Z_q\text{)} \end{cases} , \quad \text{(A-12)}$$

where $Z_q = (1 - f)Z_{j+1/2} + fZ_{j-1/2}$,

$$f = \frac{\rho_L - \rho_m}{\rho_L - \rho_U} ,$$

$$\rho_m = \alpha_j \rho_{vj} + (1 - \alpha_j)\rho_{\ell j} ,$$

$$\rho_U = \alpha_U \rho_{vj} + (1 - \alpha_U)\rho_{\ell j} , \quad \text{(A-13)}$$

$$\rho_L = \alpha_L \rho_{vj} + (1 - \alpha_L)\rho_{\ell j} ,$$

$$\alpha_L = \max (0.2, \alpha_{j-1}) ,$$

and

$$\alpha_U = \alpha_{j+1} .$$

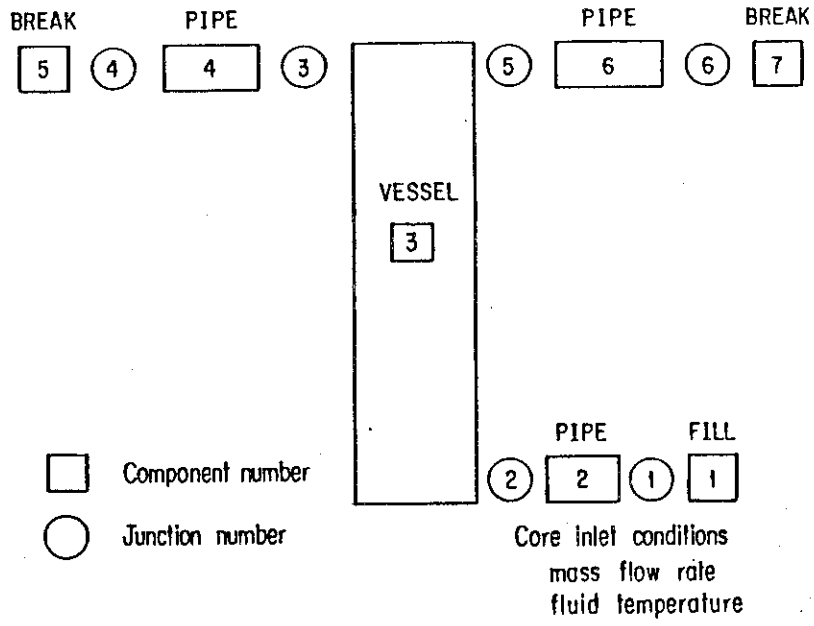

Fig. 1 TRAC schematics for CCTF core calculation.

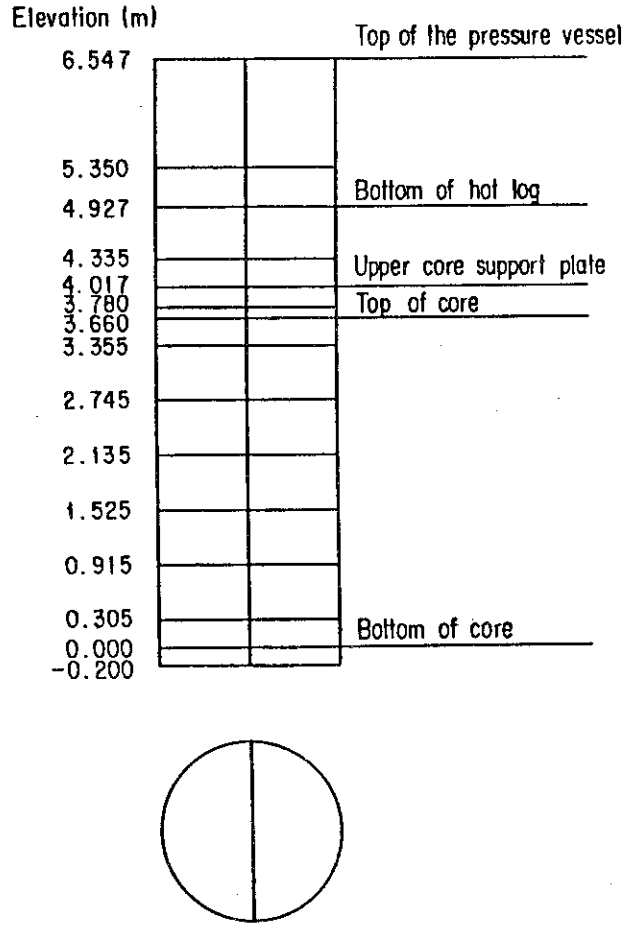

Fig. 2 Vessel noding schematic.

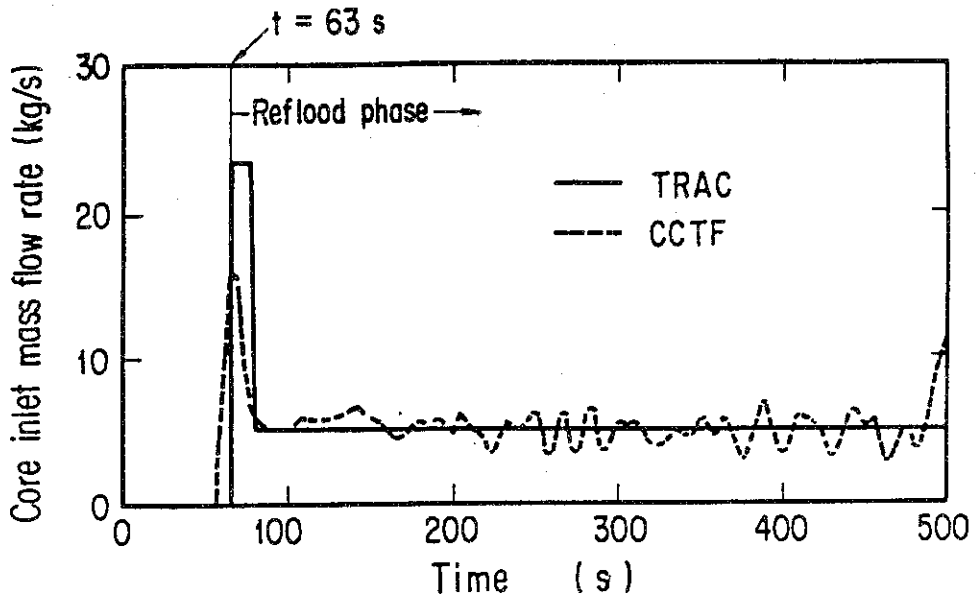

Fig. 3 Comparison of core inlet mass flow rate.

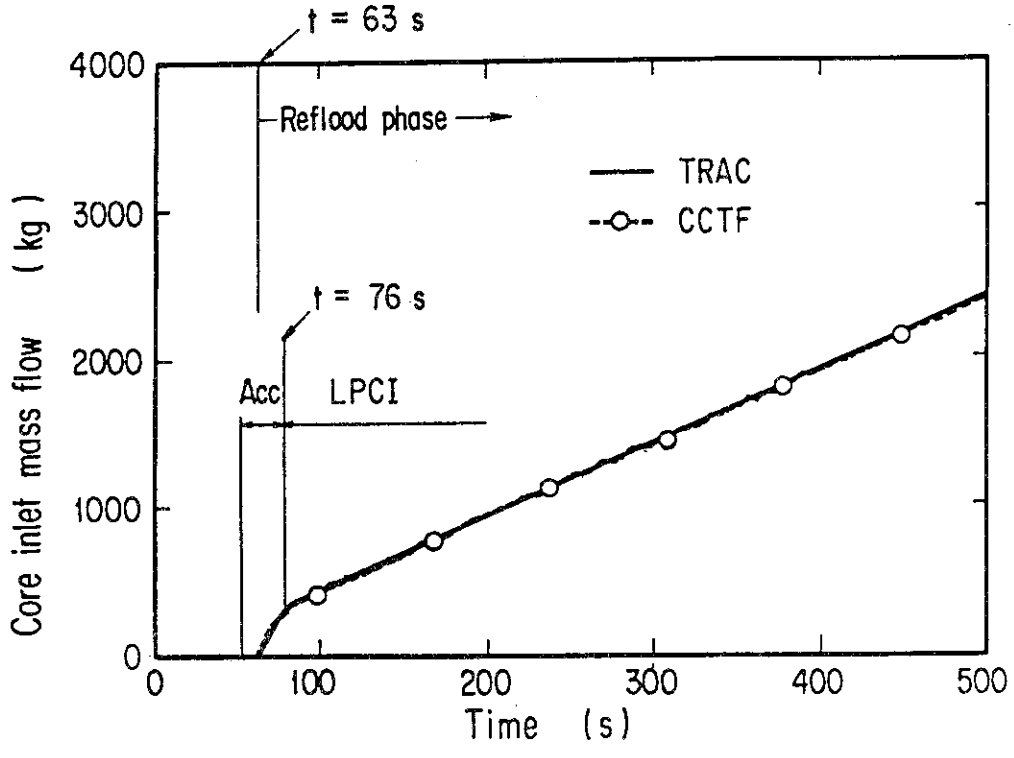

Fig. 4 Comparison of core inlet mass flow

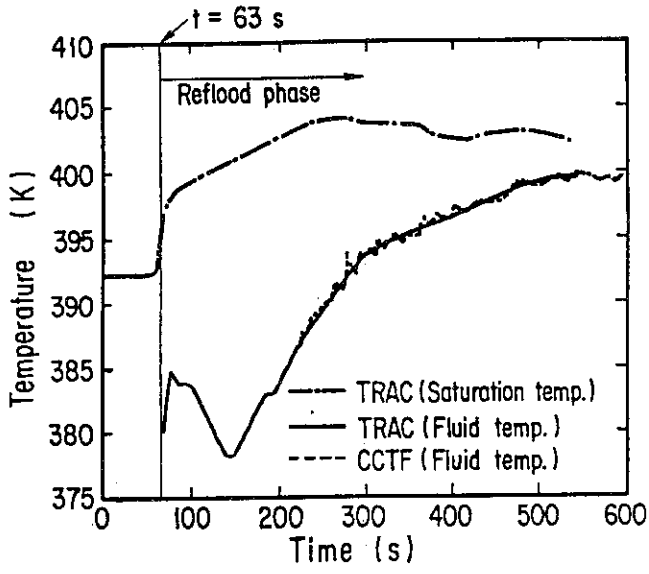

Fig. 5 Comparison of core inlet fluid temperature.

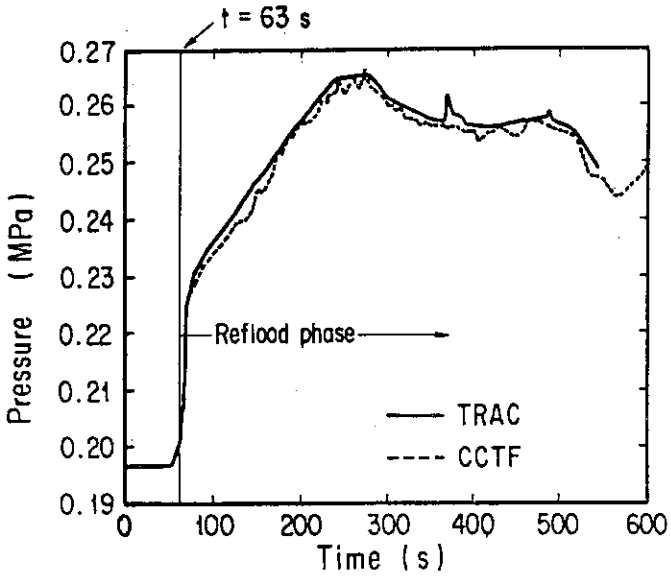

Fig. 6 Comparison of upper plenum pressure.

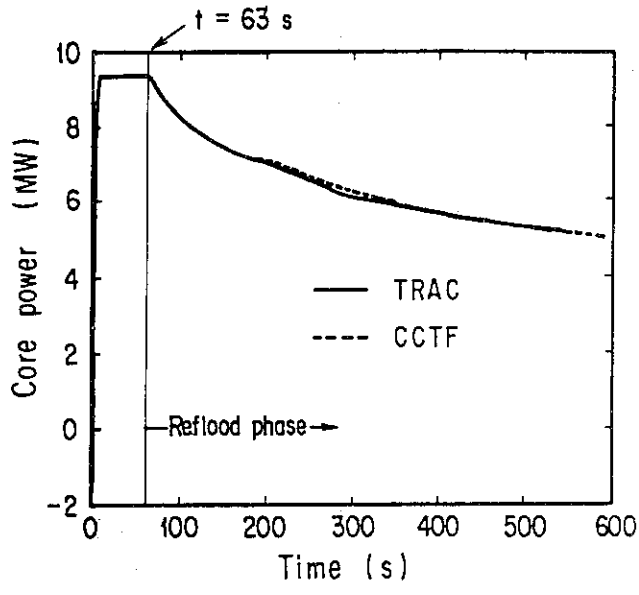

Fig. 7 Comparison of core power.

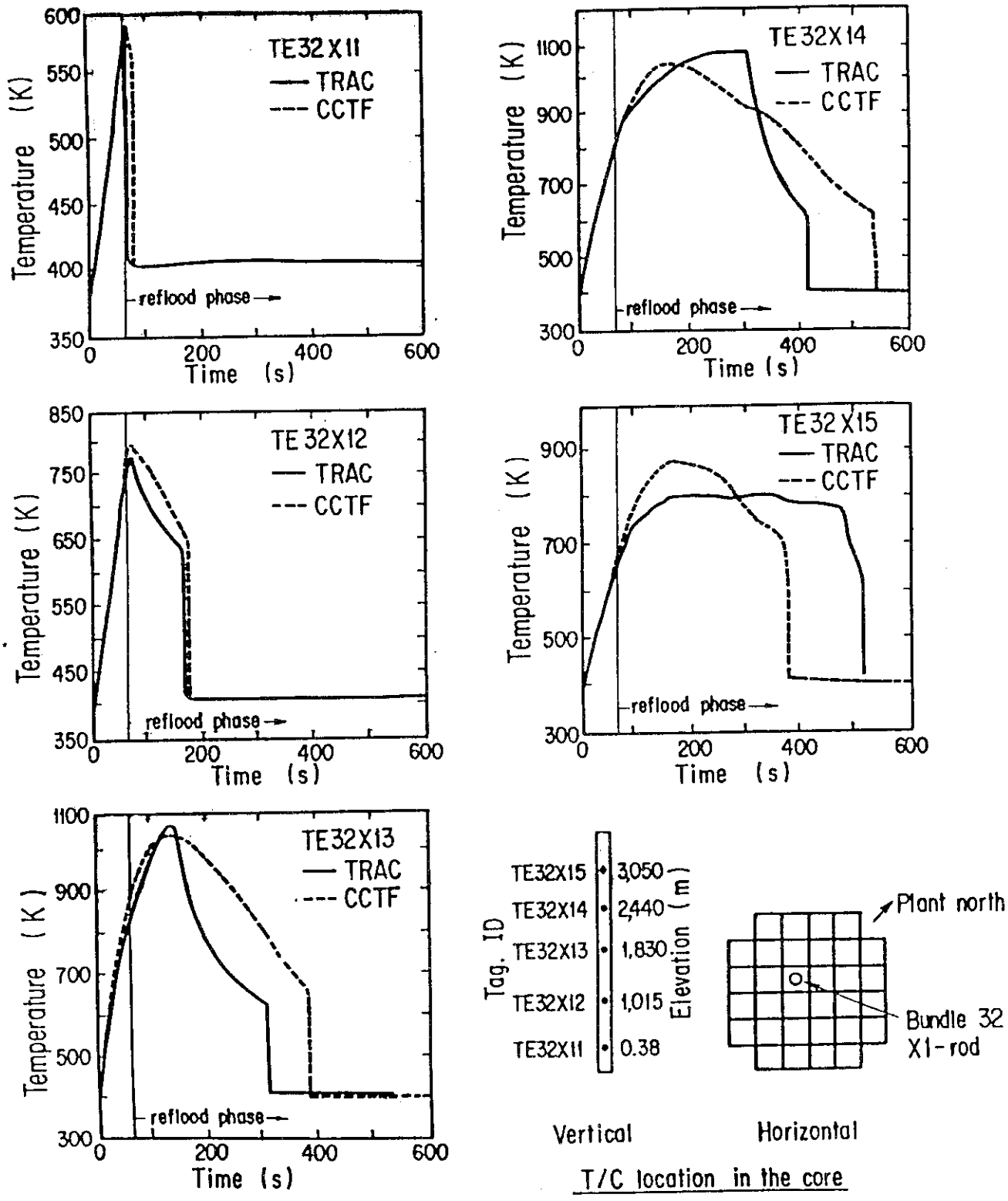

Fig. 8 Comparison of rod surface temperature histories along a high power rod in the high power region.

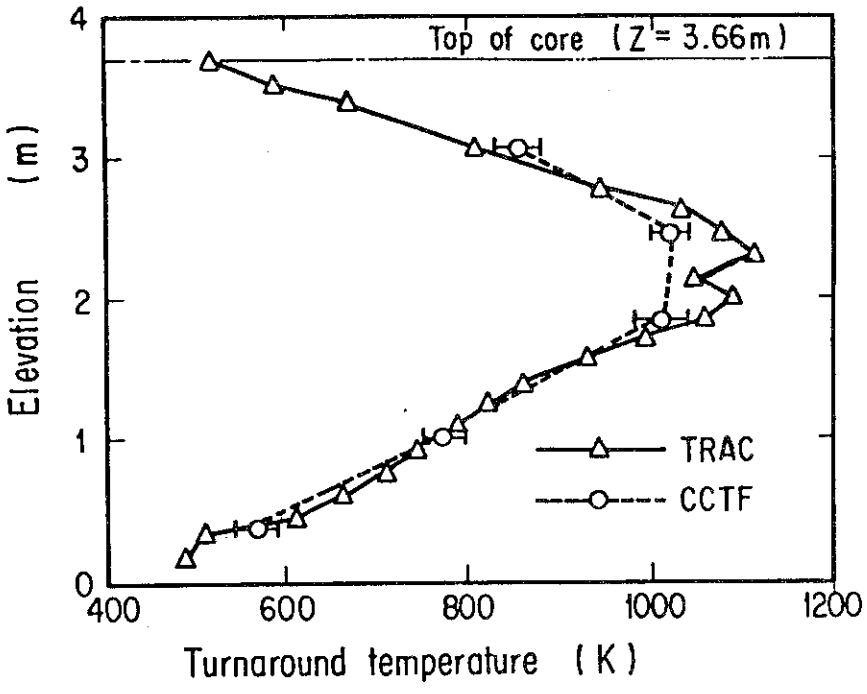

(a) High power rod in high power region

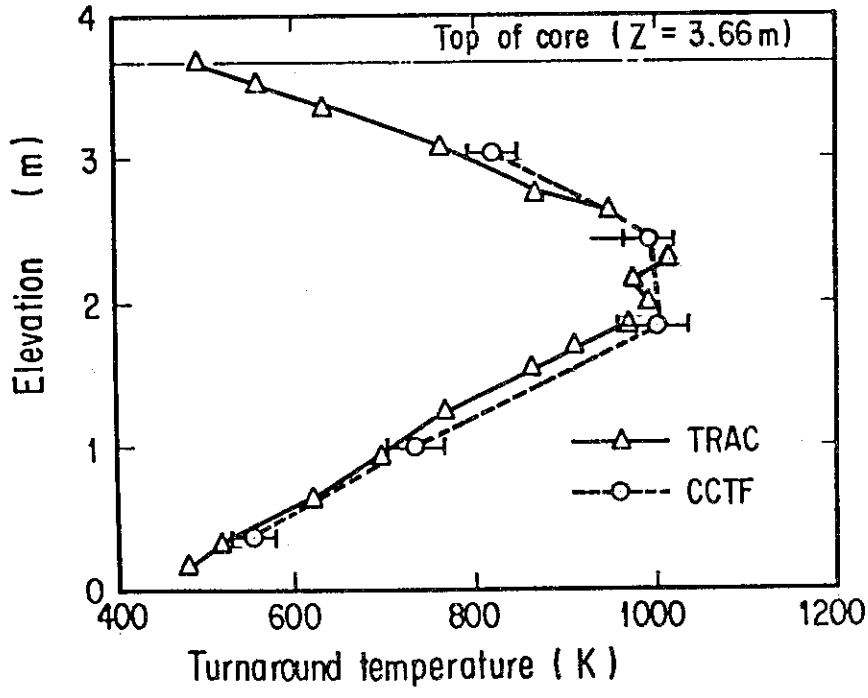

(b) Medium power rod in medium power region

Fig. 9 Comparison of turnaround temperatures between TRAC and CCTF results. (a) High power rod in the high power region (b) Medium power rod in the medium power region.

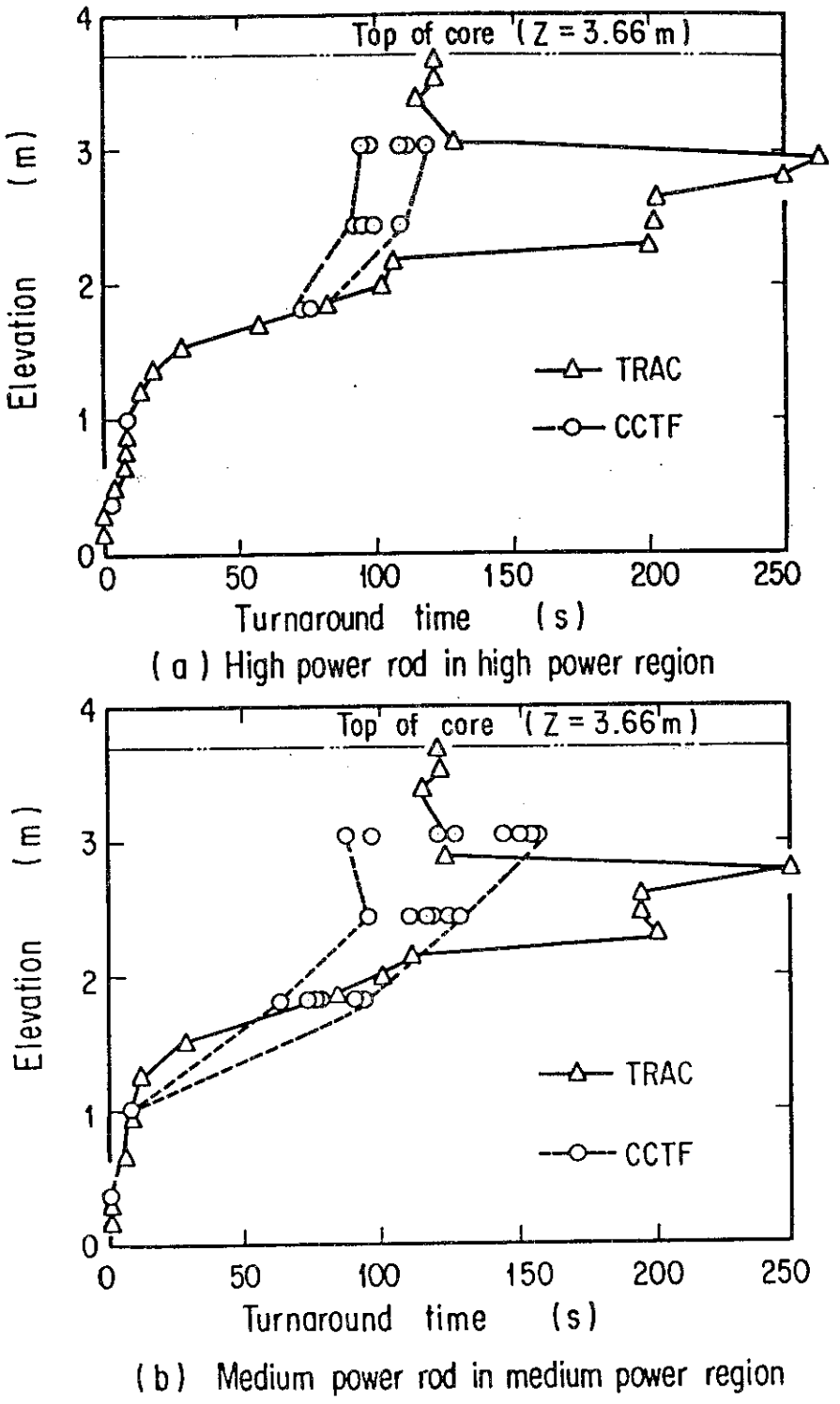

Fig. 10 Comparison of turnaround times between TRAC and CCTF results. (a) High power rod in the high power region (b) Medium power rod in the medium power region.

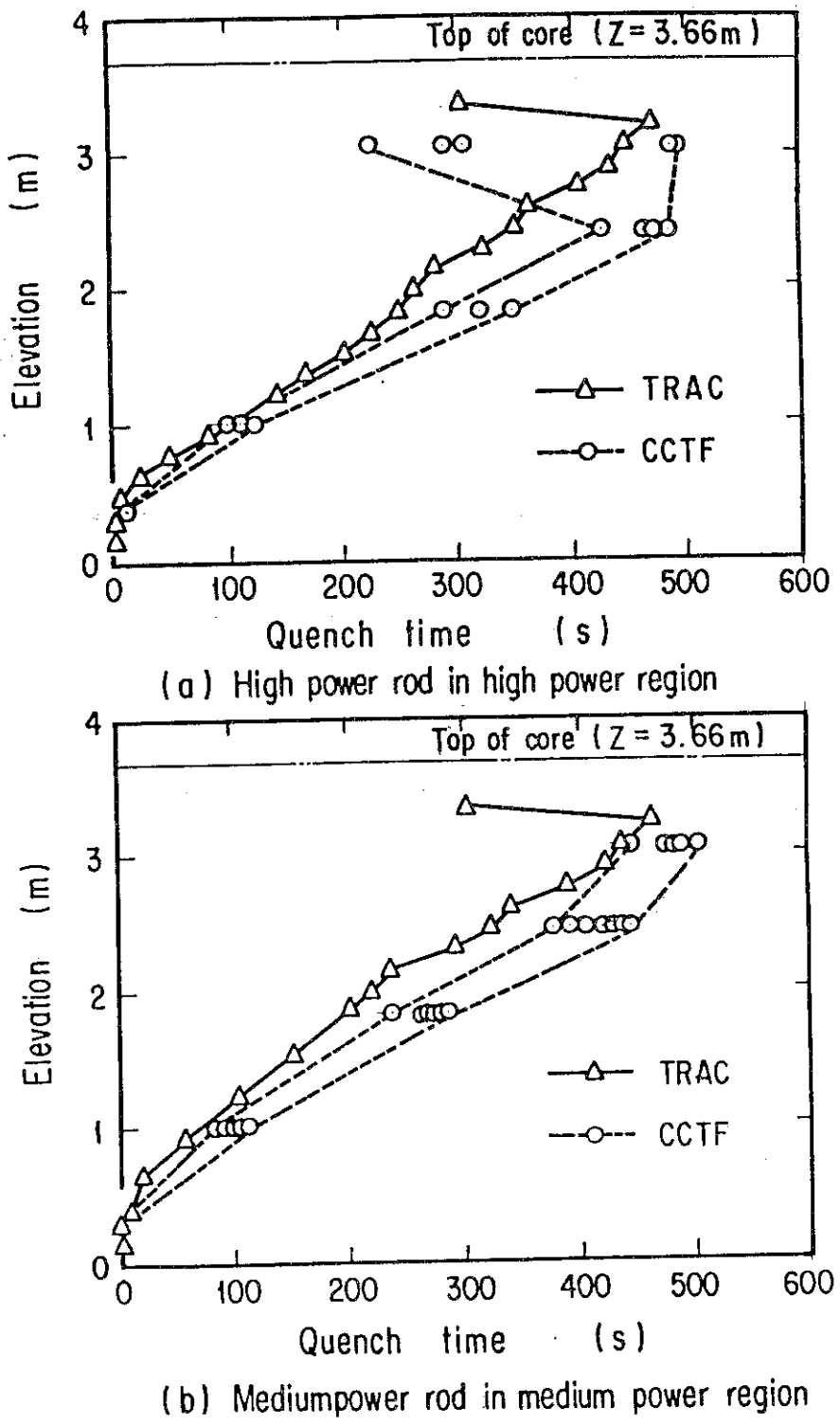

Fig. 11 Comparison of quench times between TRAC and CCTF results. (a) High power rod in the high power region (b) Medium power rod in the medium power region.

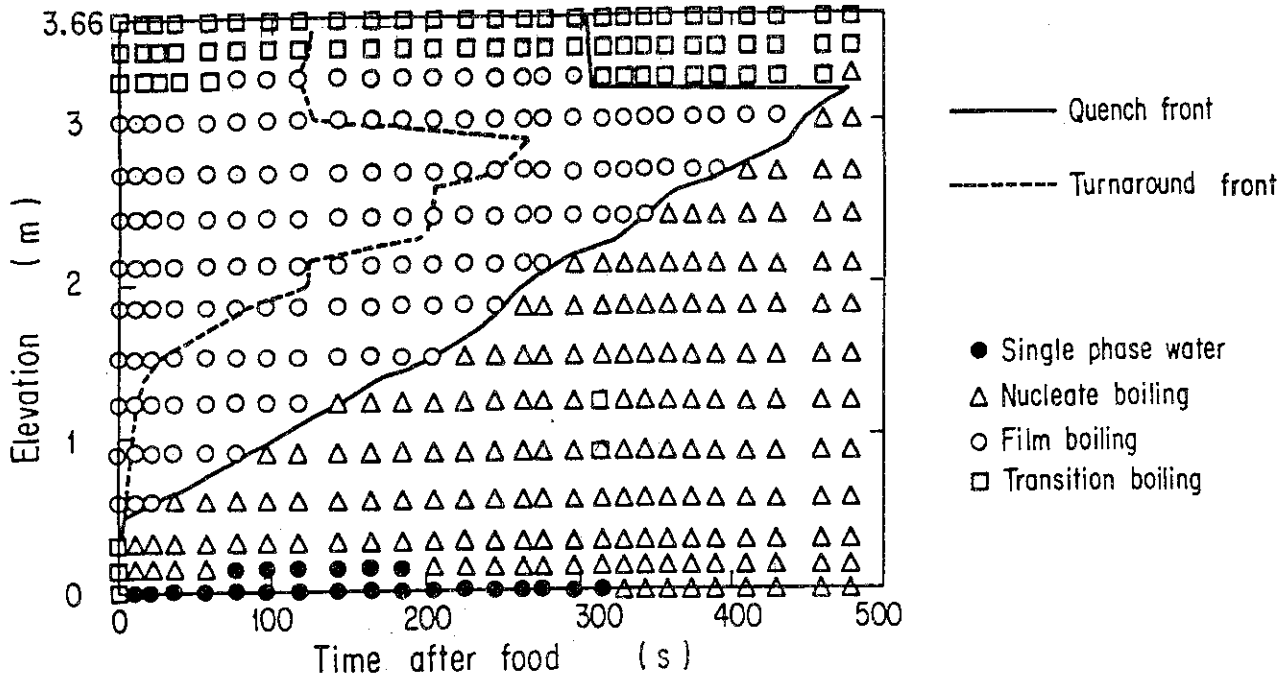

Fig. 12 Predicted wall-to-fluid heat transfer regime along a high power rod in the high power region.

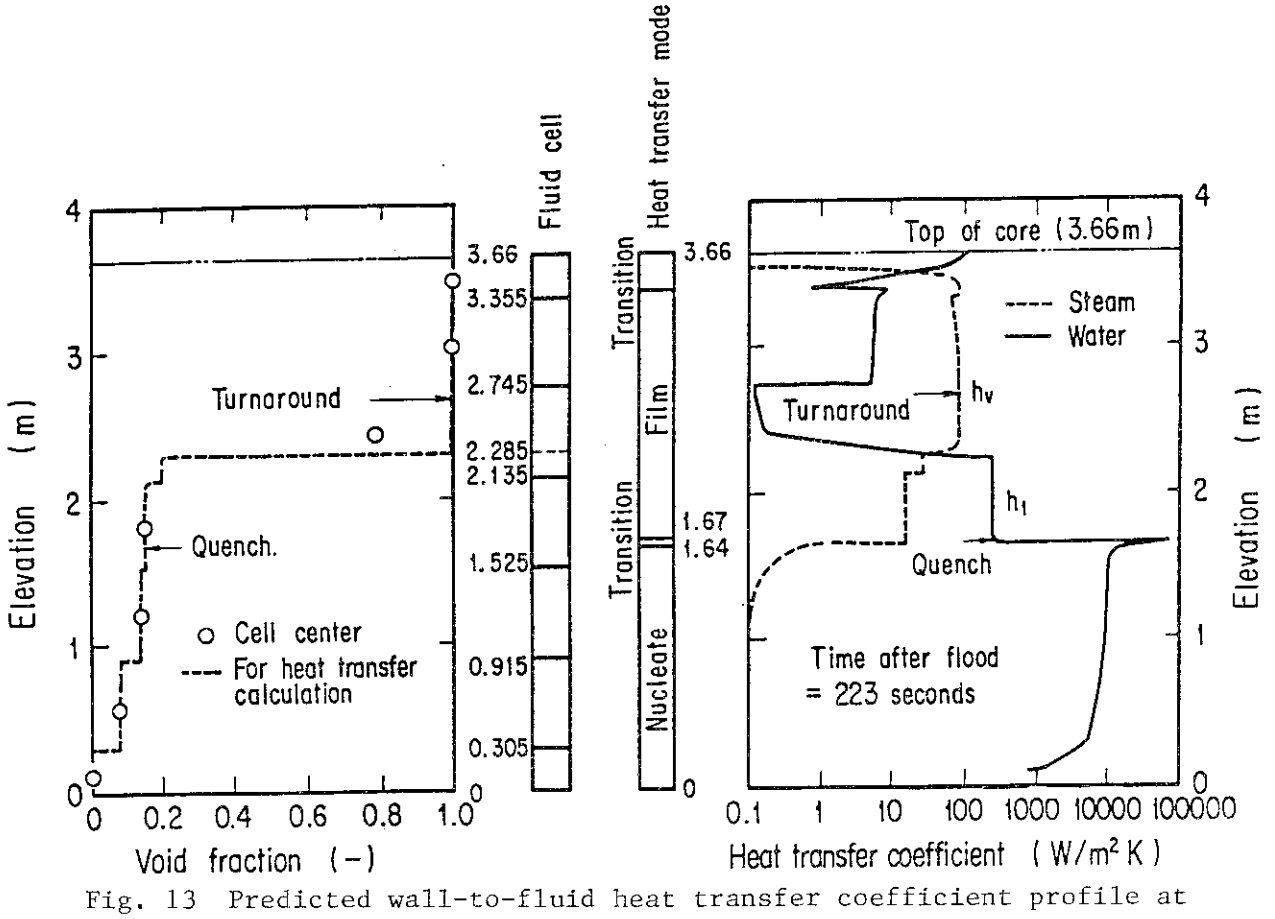

Fig. 13 Predicted wall-to-fluid heat transfer coefficient profile at 223 seconds after the reflood initiation along a high power rod in the high power region.

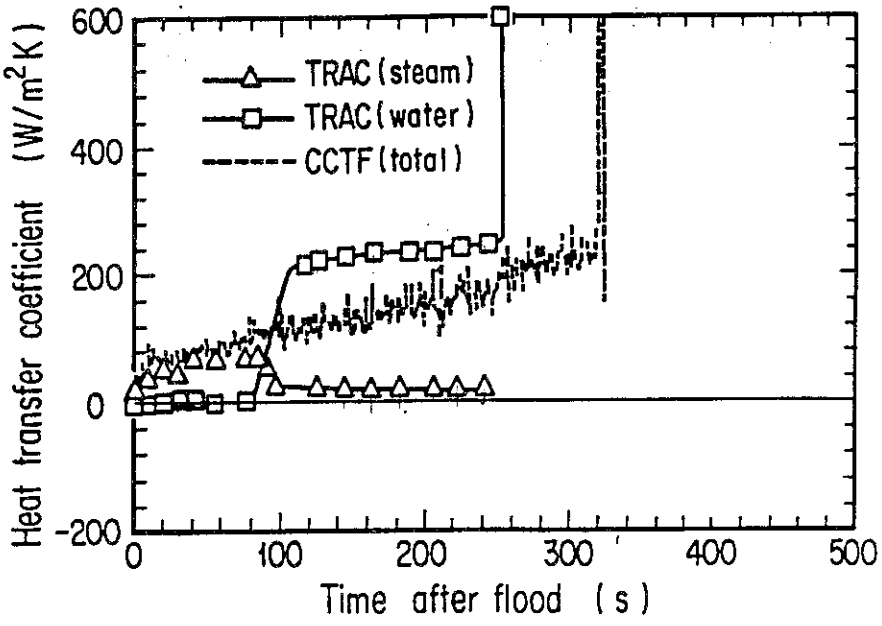

Fig. 14 Comparison of wall-to-fluid heat transfer coefficient at the midplane of a high power rod in the high power region.

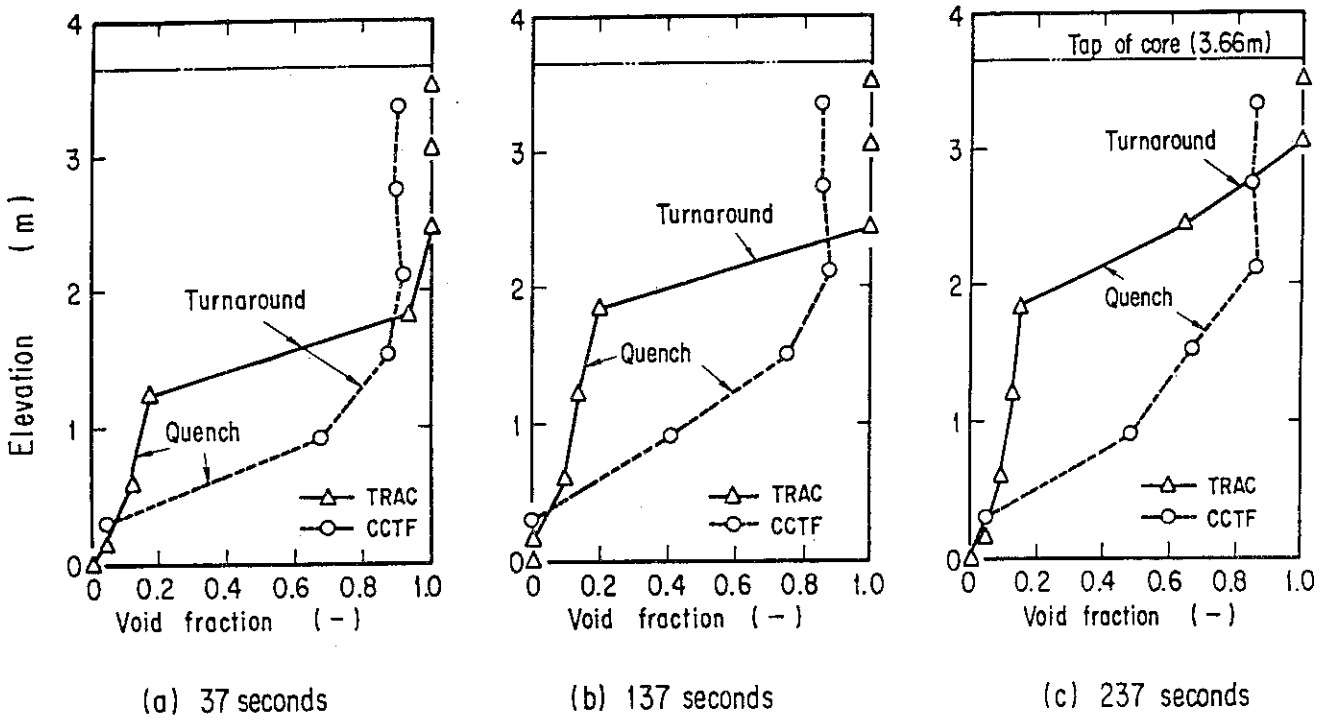

Fig. 15 Comparison of the void fraction profile in the core at 37, 137, and 237 seconds after the reflood initiation.

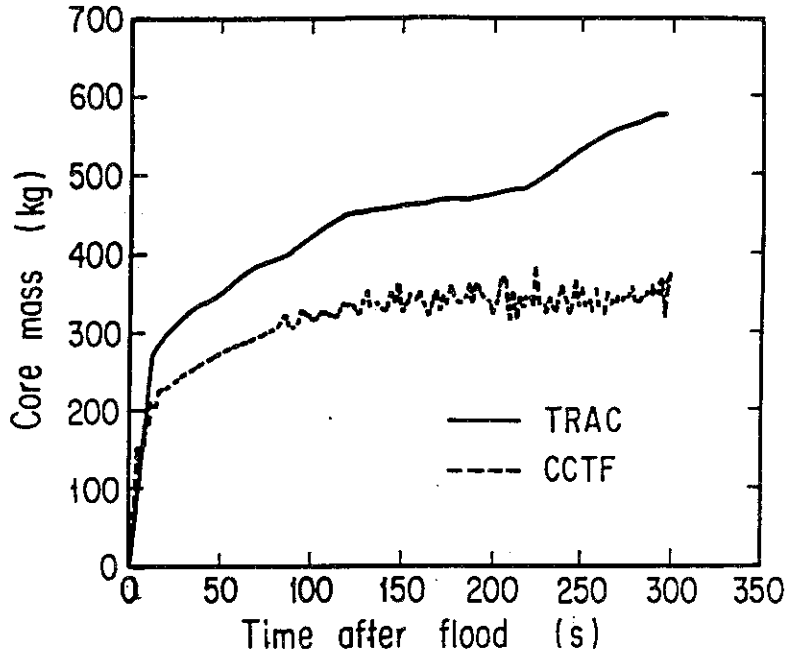

Fig. 16 Comparison of core mass between TRAC and CCTF results.

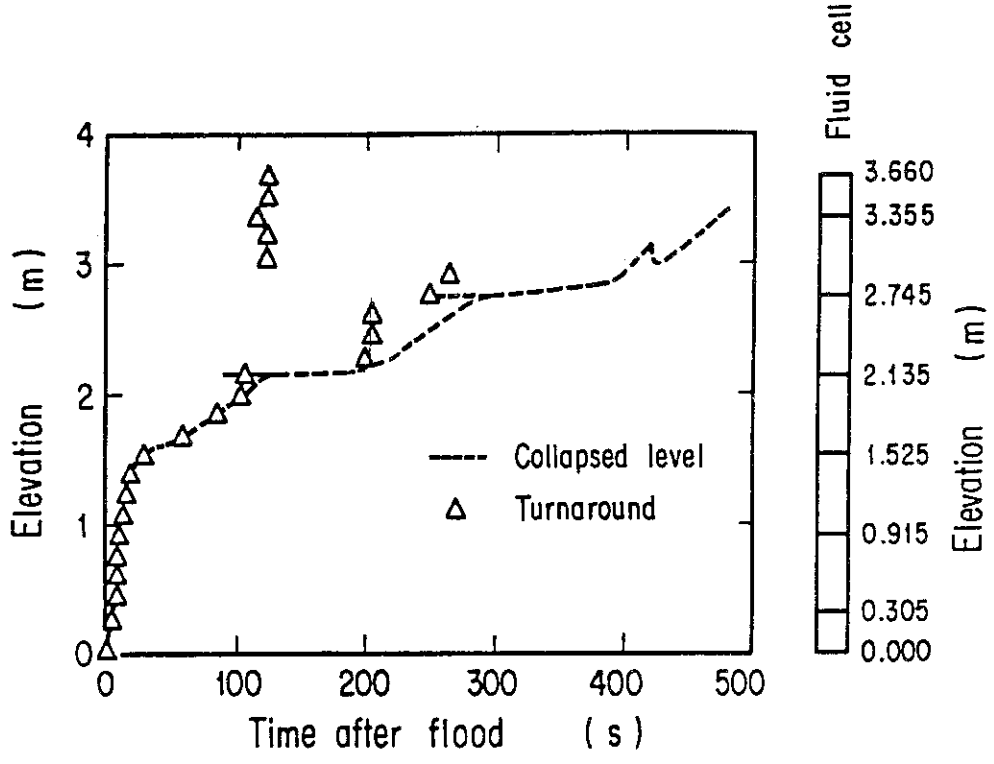

Fig. 17 Effect of the collapsed water level on the turnaround front propagation in the TRAC prediction.

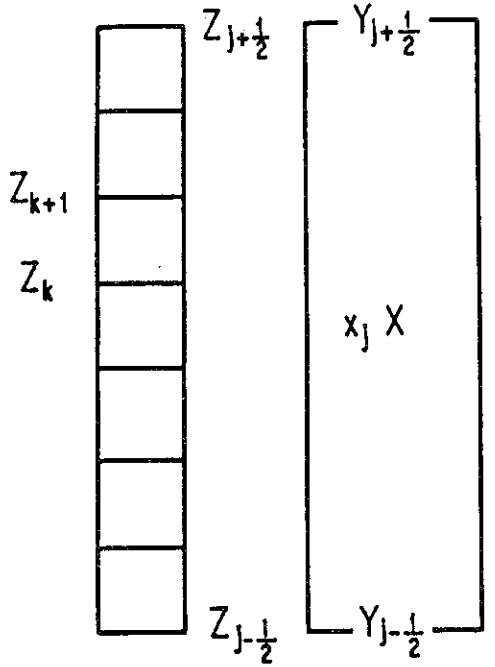

Fig. A-1

Thermo-hydraulic diameter ; D_{hj}

Pressure ; P_j

Fluid temperature ; T_{vj} , T_{lj}

Saturation temperature ; T_{satj}

Fluid property ; h_{fgj} (Latent heat)
ρ_{vj} , ρ_{lj} , ρ_{mj} (Density)
Cp_{vj} , Cp_{lj} , (Specific heat)
λ_{vj} , λ_{lj} (Thermal conductivity)
μ_{vj} , μ_{lj} (Viscosity)
σ_j (Surface tension)

Fluid velocity ; $V_{vz(j-\frac{1}{2})}$, $V_{lz(j-\frac{1}{2})}$, $V_{mz(j-\frac{1}{2})}$

Void fraction ; α_j (If Z_q is not in the cell)
α_L (If Z_q is in the cell and $Z_k < Z_q$)
α_U (If Z_q is in the cell and $Z_{k+1} > Z_q$)

Rod surface temperature ; T_{wk}

Rod property ; C_{pw} , λ_w , e_w , ρ_w
(Linear interpolation with $T_{w(j-\frac{1}{2})}$ and $T_{w(j+\frac{1}{2})}$)